Fast oxygen-enhanced multi-slice imaging of the lung using parallel acquisition techniques

Olaf Dietrich[1], Christoph Losert[1,2], Ulrike Attenberger[1], Ulrike Fasol[1], Michael Peller[1], Konstantin Nikolaou[1], Maximilian F. Reiser[1], Stefan O. Schoenberg[1]

[1] Department of Clinical Radiology – Großhadern, Ludwig Maximilian University of Munich

[2] Department of Radiotherapy and Radiation Oncology, Ludwig Maximilian University of Munich

Final version: *Magn Reson Med* 2005; **53**(6): 1317–1325. <URL:http://dx.doi.org/10.1002/mrm.20495>

Abstract

The purpose of this study was to evaluate an optimized multi-slice acquisition technique for oxygen-enhanced MRI of the lung using slice-selective inversion and refocusing pulses in combination with parallel imaging. An inversion recovery HASTE sequence was implemented with respiratory triggering to perform imaging in end-expiration and with ECG triggering to avoid image acquisition during the systolic phase. Inversion pulses and the readout of echo trains could be interleaved to decrease acquisition time. The sequence was evaluated in 15 healthy volunteers, comparing three acquisition schemes: (1) acquisition of 4 slices without parallel imaging; (2) acquisition of 4 slices with parallel imaging; (3) acquisition of 6 slices with parallel imaging. These multi-slice acquisitions were repeated 80 times with alternating inhalation of room air and oxygen. The oxygen-induced signal increase showed no significant difference with and without parallel imaging. However, only with parallel imaging the interleaved acquisition of 6 or more slices became possible, thus enabling a more complete anatomic coverage of the lung. The average required end-expiration time per repetition to acquire 6 slices could be significantly reduced from 4112 ms without to 2727 ms with parallel imaging. Total acquisition time varied between 8 and 13 minutes depending on the respiratory frequency.

Keywords:

Oxygen-enhanced lung imaging;
Parallel acquisition technique; ECG triggering;
Respiratory triggering

Corresponding author:

Olaf Dietrich, PhD
Radiological Physics
Department of Clinical Radiology – Großhadern
Ludwig Maximilian University of Munich
Marchioninistr. 15, 81377 Munich, GERMANY
Phone: +49-89-7095-3623
Fax: +49-89-7095-4627
E-mail: od@dtrx.net

Introduction

Proton MRI of the lung is considerably more difficult than MRI of most other organs due to the very low signal intensity of the lung tissue caused by its low average proton density and short T_2* relaxation time. Both properties are a consequence of the heterogeneous microstructure of the lung parenchyma which consists mainly of microscopic air-filled alveoli with a large interface between air spaces and tissue or blood; hence, large local variations of susceptibility occur within small spatial scales. In 1996, Edelman et al. (1) have suggested to use molecular oxygen as paramagnetic contrast agent for proton MRI of the lung in order to provide images with enhanced signal of the lung tissue. Averaging over all tissue compartments within a single voxel, an effective oxygen-induced T_1 reduction of about 10 % to 15 % is observed in the lung parenchyma after inhalation of pure oxygen (1–3). This change of longitudinal relaxation can be measured as signal variations in repeated T_1-weighted image acquisitions: typically a block paradigm is used consisting of alternating blocks with inhalation of room air (21 % oxygen) and pure oxygen. Since the underlying signal mechanism is based on an increased oxygen concentration in the capillary blood of the lung, oxygen-enhanced lung imaging provides combined information about three physiological parameters: sufficient ventilation and perfusion in combination with oxygen diffusion from the alveoli into the capillaries of the lung are required for signal enhancement (1, 3). Thus, oxygen-enhanced lung MRI can be regarded as imaging of "lung function" understood as the combination of these three parameters.

Oxygen-enhanced lung imaging has been evaluated in several studies demonstrating a good correlation between MRI parameters and conventional methods of lung diagnostics such as evaluation of the diffusion capacity of carbon monoxide (DLCO), the forced expiratory volume in 1 second (FEV), or results of ventilation scintigraphy. Ohno et al. (4, 5) examined patients with lung cancer and with lung emphysema and demonstrated good correlation of maximum signal enhancement in oxygen-enhanced MRI on the one hand and FEV and DLCO on the other hand. Another study in patients with various pulmonary diseases also showed a good correlation between the signal slope after switching the gas supply to pure oxygen and the DLCO (6). However, almost all oxygen-enhanced imaging studies we are aware of were performed with non-selective inversion or refocusing pulses such that an interleaved inversion and acquisition of multiple slices is not possible. Hence, either single-slice imaging methods were used or the total duration of acquisition was considerably prolonged in order to acquire up to four slices.

Recent improvements in imaging technique known as "partially parallel acquisition" or "integrated parallel acquisition techniques" (iPAT) have been developed since the late 1990s with the aim to accelerate image acquisition (7–9). The underlying idea is to use several parallel receiver coil elements with spatially different coil sensitivity profiles to acquire multiple data sets with reduced k-space sampling density in phase-encoding direction. These data sets are used to calculate a single image corresponding to a fully sampled k-space during post-processing. The purpose of this work was to provide a robust multi-slice acquisition technique for oxygen-enhanced lung imaging by combining parallel imaging with a new ECG and respiratory triggering scheme and slice-selective RF pulses for inversion and refocusing. The aim was to achieve a more complete coverage of the lung with up to 6 coronal slices without prolongation of the total duration of the measurement and, thereby, provide the means for an integration of oxygen-enhanced lung imaging into clinical routine protocols of lung MRI.

Methods

A multi-slice Inversion Recovery Half-Fourier Acquired Single-shot Turbo spin Echo (IR-HASTE) sequence was used for all imaging experiments described below. The most important feature of this sequence is the newly implemented simultaneous use of respiratory and ECG triggering combined with a flexible acquisition scheme that allows interleaving of inversion pulses and the readout of echo trains of multiple slices as shown in Fig. 1. Respiratory triggering is used to perform imaging in end-expiration during slow but free breathing of the examined subject. ECG triggering is employed to provide constant cardiac phases for all

acquisitions of each slice and to avoid image acquisition during the systolic phase.

The triggering algorithm is implemented as a 2-stage scheme that first waits for the desired respiratory phase before the actual cardiac triggering is performed. For oxygen-enhanced lung imaging, the first stage of the triggering algorithm waits for almost full expiration of the subject. Then the evaluation of the ECG signal starts (second stage); at the detection of the next R-wave of the ECG signal, a short-time average of the heart rate is requested from the physiological measurement unit (PMU) of the MRI system. The current heart rate is used to calculate a delay T_D such that the following acquisitions of image data (readout of HASTE echo train) are performed in the diastolic phase. After this delay, the inversion pulses are applied followed by the actual readout of the echo trains after the inversion time T_{Inv}. Since the combined duration of the echo trains of all slices can be longer than the diastolic interval, a separation of the readouts into two subsequent RR intervals is typically selected; this scheme is called "interleaved acquisition" and is shown in Fig. 1a (note that the term "interleaved" does *not* refer to the order of acquired slice positions, but to the process of interleaving two blocks of inversion pulses and HASTE readouts in order to fit all readouts into the diastolic phases). It depends on the heart rate of the examined subject and on the timing parameters, i.e. the inversion time, the duration of the HASTE readout, and the number of acquired slices whether an interleaved acquisition is possible or not. If the current RR interval T_{RR} determined by the PMU is too short or too long for the interleaved scheme, the triggering algorithm switches automatically to a non-interleaved scheme (Fig. 1b). In this case, the end-expiration time T_{Exp} required for a motion-free acquisition is considerably longer. Examples of the calculation of the delay and the selection of the interleaved or non-interleaved acquisition scheme are also given in Fig. 1a and 1b.

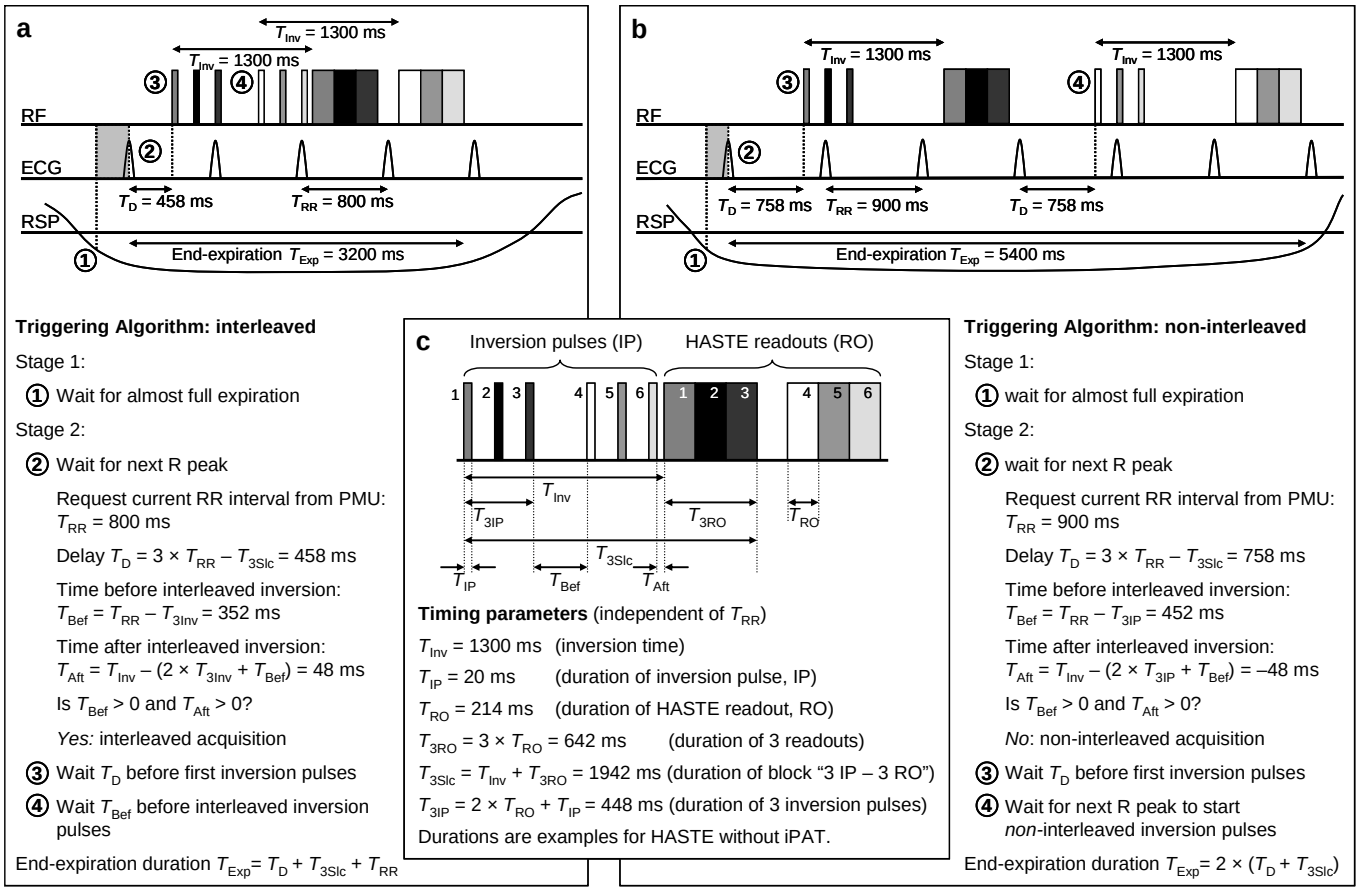

Figure 1: Triggering algorithm; diagrams show RF pulses (inversion and HASTE readout echo train; the 6 different slices are represented by different shades of gray), ECG, and respiratory signal (RSP). Depending on the timing parameters and the RR interval T_{RR}, acquisition can be interleaved (T_{RR} = 800 ms, Fig. 1a) or non-interleaved (T_{RR} = 900 ms, Fig. 1b). Common timing parameters that are independent of the heart rate are shown in Fig. 1c (this is a magnification of the RF pulses in Fig. 1a); the sequence parameters are taken from the non-iPAT IR-HASTE sequence.

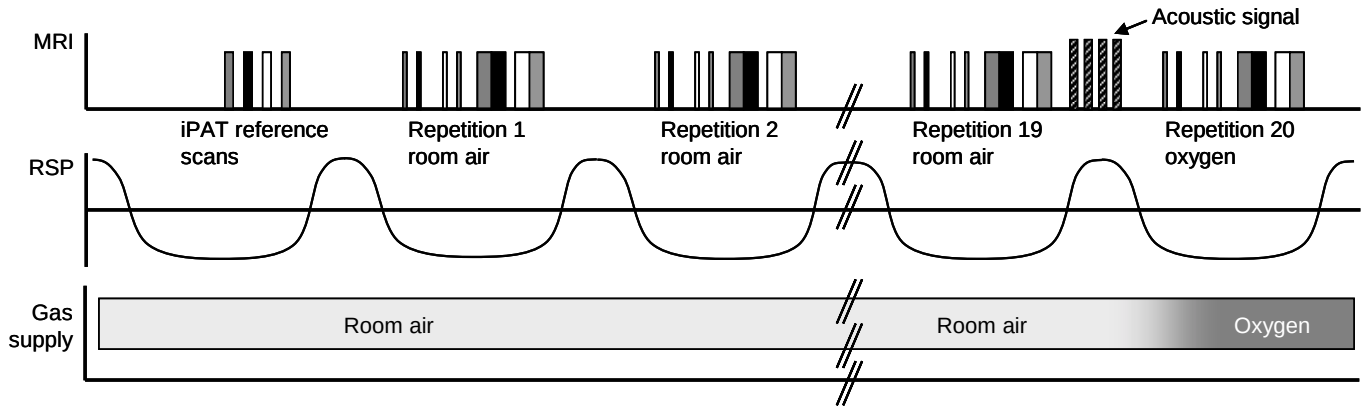

Figure 2: Time course of measurements; MRI events (gradients (hatched) and RF pulses; 4 different slices are represented by different shades of gray), respiratory signal (RSP), and gas supply are shown. Data acquisition is performed in end-expiration. Note the gradient signal indicating acoustically the change of gas supply after measurement 19, and the subsequent change from room air to oxygen.

Our IR-HASTE sequence can be run with conventional imaging and with parallel imaging in order to reduce the echo train length and thus the HASTE readout duration. The acquisition of the coil sensitivity profiles required for the iPAT reconstruction is integrated into the sequence in the form of additionally acquired reference lines in the center of k-space; thus, a low-resolution image without aliasing artifacts can be reconstructed for each receive coil element. Since acquiring these reference lines is time-consuming and increases both the echo train length and minimum echo time, the acquisition of these extra lines has been moved to the beginning of the pulse sequence and is thus performed only once for all repetitions of a measurement (Fig. 2). A similar respiratory and ECG triggering algorithm as for the actual acquisitions is used for the reference scans to provide coil sensitivity profiles for each slice that are acquired in the same respiratory phase as the following HASTE data readouts. The iPAT reconstruction is performed using the GRAPPA algorithm (9) and the coil sensitivity profiles are based on the 24 central k-space lines.

The IR-HASTE sequence was implemented on a 1.5 T whole-body MR system (Magnetom Sonata Maestro Class, Siemens Medical Solutions, Erlangen, Germany) with a high-performance gradient system providing a maximum gradient strength of 40 mT/m and a maximum gradient slope of 200 mT/(m ms). We used a dedicated iPAT surface coil system that consists of 12 coil elements (6 posterior and 6 anterior); 8 of these 12 elements are combined in pairs of 2 such that together with the remaining 4 elements the coil system matches the 8 receiver channels of the MR system. T_1-weighting of the IR-HASTE sequence was achieved with an optimized inversion time (3) of 1300 ms, a repeat time of one respiratory cycle (thus ranging between about 5 s and 10 s), and an echo spacing of 2.7 ms. To minimize artifacts, a linear k-space readout in phase-encoding direction is used giving a (minimum) echo time of 19 ms without iPAT and 11 ms with iPAT. We acquired a 128×128 matrix with a field of view of 400×400 mm^2, a slice thickness of 8 mm, and a gap between the slices of 16 mm. To reduce perfusion effects and signal alterations due to the inflow of non-inverted spins, the thickness of the slice-selective inversion pulse was set to 16 mm, i.e. twice the thickness of the imaging slice. The image acquisition was repeated 80 times in total, divided into 4 blocks of 20 repetitions each. The subjects were administered room air in the first and third block, and oxygen in the second and fourth block.

A respiratory mask covering mouth and nose was used to administer either room air or oxygen with a gas flow of approximately 20 L/min; the gas supply was changed manually after 20, 40, and 60 measurements. As shown in Fig. 2, four additional gradient lobes are inserted into the pulse sequence after repetition 19, 39, and 59 to indicate acoustically that the gas supply is to be changed. These gradients have no influence on the actual imaging, since the signal of following acquisition depends only on the longitudinal magnetization.

Image post-processing consisted of four steps: a preliminary selection of the repetitions to be evaluated, retrospective motion correction, calculation of the relative signal increase, and a careful spatial low-pass filtering of the resulting data. As first step of post-

processing, those 5 repetitions immediately following each change of gas supply were discarded from further evaluation in order to avoid the intermediary signal during the oxygen wash-in and wash-out periods. The retrospective motion correction algorithm requires the definition of a region over the diaphragm and then compares the vertical diaphragm position in the remaining 65 repetitions with the diaphragm position in an average image (pixel intensities in this average image were calculated as pixel-by-pixel median of all 80 repetitions). Only acquisitions with identical diaphragm position within 1 pixel (3.1 mm) are accepted for further processing. All accepted images of room air measurements on the one hand and of oxygen measurements on the other hand are averaged and a map of relative signal increase $\Delta S_{rel} = (S_{oxygen}–S_{air})/S_{air}$ is calculated. To reduce the influence of statistical noise, the maps are low-pass filtered before visualization using a 3×3 Gauss filter with a standard deviation of 1 pixel.

We examined 15 healthy volunteers (8 male, 7 female) aged between 20 and 37 years; the volunteers gave written informed consent to participate in the study, which had local Ethics Committee approval. Three different acquisition schemes were compared. Scheme 1: acquisition of 4 slices without iPAT (8 volunteers, mean age 24.4 years); Scheme 2: acquisition of 4 slices with iPAT (11 volunteers, mean age 25.7 years); Scheme 3: acquisition of 6 slices with iPAT (5 volunteers, mean age 33.8 years). Before the actual acquisition, the triggering scheme was explained to the volunteers and they were asked to try to adapt the duration of their end-expiration period to the duration of the sequence readout. Then, 6 repetitions of the acquisition were used as training. Comparing the online display of the respiratory signal with the actual training acquisitions, feedback was given to the volunteers to improve their respiratory timing if necessary.

In 3 of the volunteers (#10, #14, #15) the sequence was applied both with slice-selective and non-selective inversion pulses in order to evaluate the effect of the slice-selective inversion in comparison with the established non-selective preparation. To obtain a non-selective inversion, all but one inversion pulses were removed without changing the timing of the sequence; the remaining inversion pulse was applied with an inversion slice thickness of 1600 mm, i.e. as virtually non-selective pulse. Only the slice belonging to this remaining inversion pulse was evaluated, since the other slices were now prepared with different inversion times. The T_1-weighted images were compared for arterial enhancement due to inflow effects and the oxygen-induced signal increase was quantitatively evaluated for both measurements.

Statistical evaluation of the measurements included the manual segmentation of the lung in all 4 or 6 slices, and the calculation of the mean signal increase averaged over all slices in each subject. Additionally, the (spatial) standard deviation of the signal increase was determined in each subject as a measure of signal homogeneity in the lung. These data and also the fraction of images accepted by the motion correction were compared in all 3 acquisition schemes using the Wilcoxon two-sample test.

Results

Figure 3 shows examples of the calculated maps of oxygen-induced relative signal increase without and with iPAT, as well as an example of the signal time course of all slices in one volunteer. As listed in Table 1, the signal increase was larger in most volunteers with iPAT than without; however, the difference of the mean values of relative signal increase is not significant when comparing the acquisitions with 4 slice (scheme 1 and scheme 2, $p \approx 0.09$) or the acquisitions with iPAT (scheme 2 and scheme 3, $p \approx 0.44$). A significant difference is seen in comparison of scheme 1 (no iPAT, 4 slices) and scheme 3 (iPAT, 6 slices), with $p \approx 0.03$. The averaged signal increase ranges between 8.9 % (standard deviation over all volunteers: 2.7 %) in scheme 1 and 13.1 % (3.6 %) in scheme 3. The (spatial) standard deviation of the relative signal increase within each single slice is similar without (4.8 %) and with iPAT (5.8 % in scheme 2, 5.2 % in scheme 3).

In Fig. 4, the measurements with non-selective and slice-selective inversion are compared. The T_1-weighted images show similar features with both techniques; in particular, an enhancement of the pulmonary vessels is seen in all acquisitions, although it appears slightly more prominent after slice-selective preparation. The maps of relative signal enhancement and the corresponding data in Table 2 show more heterogeneous results: In volunteer #10, the maps differ obvi-

ously; the pulmonary vessels appear dark with slice-selective inversion whereas with non-selective inversion only the central parts of the vessels show low enhancements. However, the signal increase in the peripheral lung parenchyma is very similar with both techniques. In volunteer #14, the spatial distribution of signal enhancement is very similar with both techniques, however, the absolute value of the enhancement in this slice is considerably higher with non-selective (27.0 %) than with slice-selective (16.7 %) preparation. In volunteer #15, signal enhancement is more heterogeneous with non-selective than with slice-selective inversion whereas the averaged relative signal increase is almost identical.

Using iPAT, the number of echoes required for the acquisition of a 128×128 matrix with a HASTE sequence could be reduced from 72 to 36, resulting in a reduced minimum echo time of 11 ms instead of 19 ms without iPAT; the total readout time could be decreased from 214 ms/slice to 115 ms/slice including the time for signal excitation and spoiler gradients. Visually, we did not observe manifest differences in image quality of the T1-weighted acquisitions without and with iPAT, but image blurring appeared generally reduced with iPAT. There were no visible reconstruction artifacts due to the GRAPPA reconstruction algorithm.

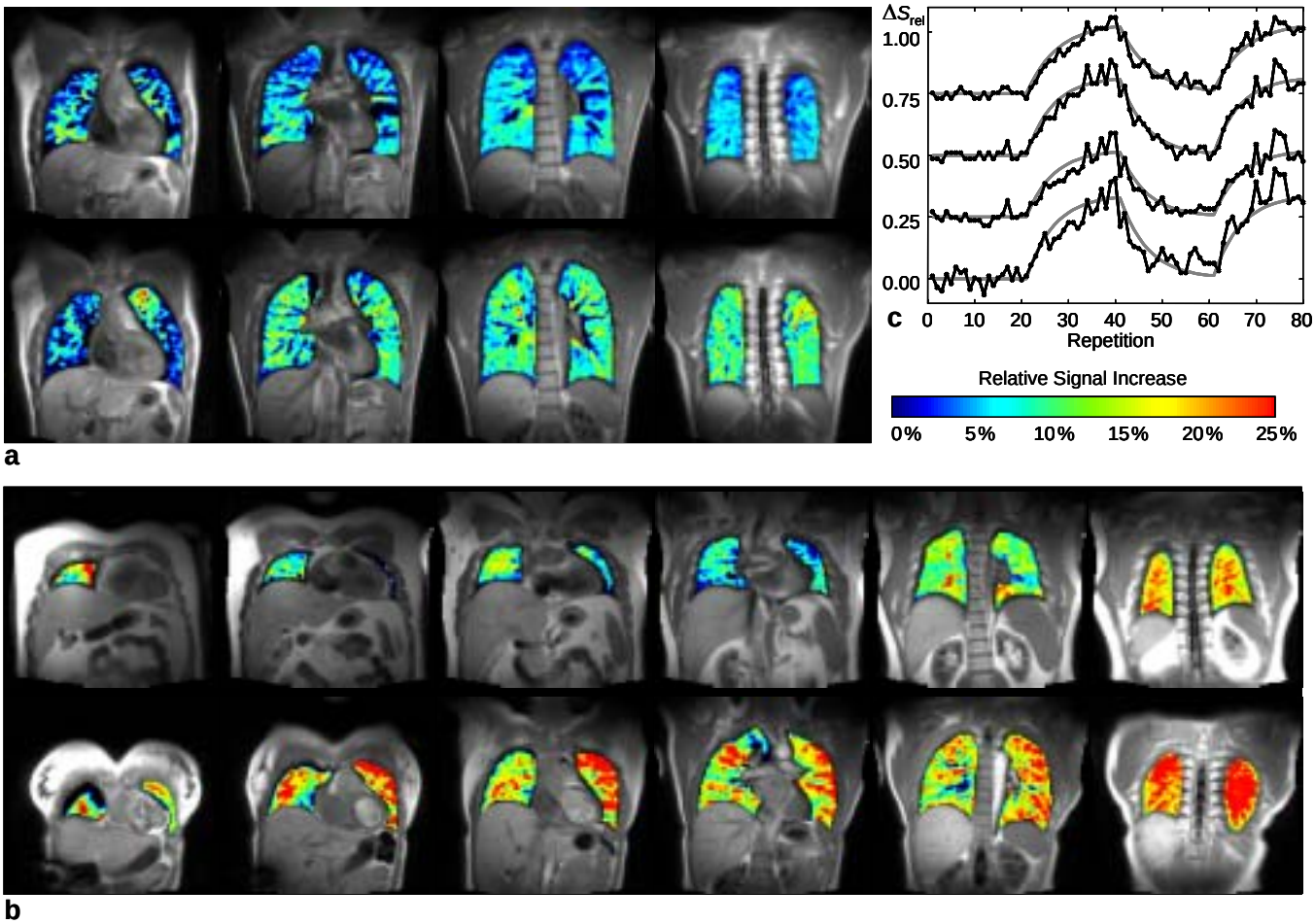

Figure 3: Examples of parameter maps displaying the oxygen-induced relative signal increase in the lung. (a) Volunteer #10; data calculated from acquisitions without iPAT (top row) and with iPAT (bottom row). (b) Acquisition of 6 slices in volunteer #12 (top row) and volunteer #13 (bottom row). (c) Time course of relative signal increase of 4 slices in volunteer #13 (acquisition scheme 2, iPAT, 4 slices). The data of the 4 slices are separated by an additional offset of 0.25; the most anterior slice is shown at the top. The data is fitted to an exponential model of oxygen wash-in and wash-out.

Table 1: Results of oxygen-enhanced imaging.

		Scheme 1: 4 slices, no iPAT				Scheme 2: 4 slices, iPAT				Scheme 3: 6 slices, iPAT			
Volunteer	Age, Sex	Relative signal increase	Std. dev. of signal increase	Trigger success room air	Trigger success oxygen	Relative signal increase	Std. dev. of signal increase	Trigger success room air	Trigger success oxygen	Relative signal increase	Std. dev. of signal increase	Trigger success room air	Trigger success oxygen
#1	23, m	–	–	–	–	16.7 %	6.3 %	67 %	69 %	–	–	–	–
#2	24, f	10.0 %	3.4 %	100 %	100 %	17.0 %	4.9 %	98 %	100 %	–	–	–	–
#3	23, m	6.1 %	6.8 %	26 %	34 %	9.7 %	12.0 %	22 %	17 %	–	–	–	–
#4	24, m	7.1 %	4.6 %	97 %	96 %	9.3 %	5.7 %	97 %	98 %	–	–	–	–
#5	26, f	13.9 %	6.5 %	92 %	87 %	–	–	–	–	–	–	–	–
#6	21, f	11.2 %	4.3 %	95 %	87 %	11.0 %	4.1 %	89 %	95 %	–	–	–	–
#7	25, f	9.2 %	6.4 %	70 %	77 %	–	–	–	–	–	–	–	–
#8	24, f	–	–	–	–	10.3 %	6.8 %	57 %	52 %	–	–	–	–
#9	20, f	7.4 %	2.3 %	97 %	100 %	6.7 %	2.7 %	99 %	100 %	–	–	–	–
#10	32, m	6.5 %	3.7 %	100 %	100 %	8.9 %	4.5 %	100 %	100 %	10.2 %	5.3 %	98 %	99 %
#11	26, m	–	–	–	–	12.9 %	5.6 %	100 %	99 %	–	–	–	–
#12	31, m	–	–	–	–	9.7 %	5.6 %	54 %	60 %	13.0 %	4.6 %	65 %	48 %
#13	35, f	–	–	–	–	21.9 %	5.4 %	92 %	96 %	18.4 %	6.5 %	94 %	97 %
#14	34, m	–	–	–	–	–	–	–	–	14.5 %	5.4 %	99 %	100 %
#15	37, m	–	–	–	–	–	–	–	–	9.5 %	4.0 %	98 %	97 %
Mean[a]		8.93 %*	4.76 %	84.8 %	85.20 %	12.19 %	5.78 %	79.6 %	80.4 %	13.12 %*	5.16 %	91.1 %	88.1 %
Std.dev.[a]		2.68 %	1.67 %	25.8 %	22.17 %	4.53 %	2.33 %	25.9 %	27.6 %	3.58 %	0.96 %	14.5 %	22.6 %

[a] Mean value and standard deviation calculated over all volunteers; * denotes a significant (p<0.05) difference.
– denotes measurements not performed in this volunteer.

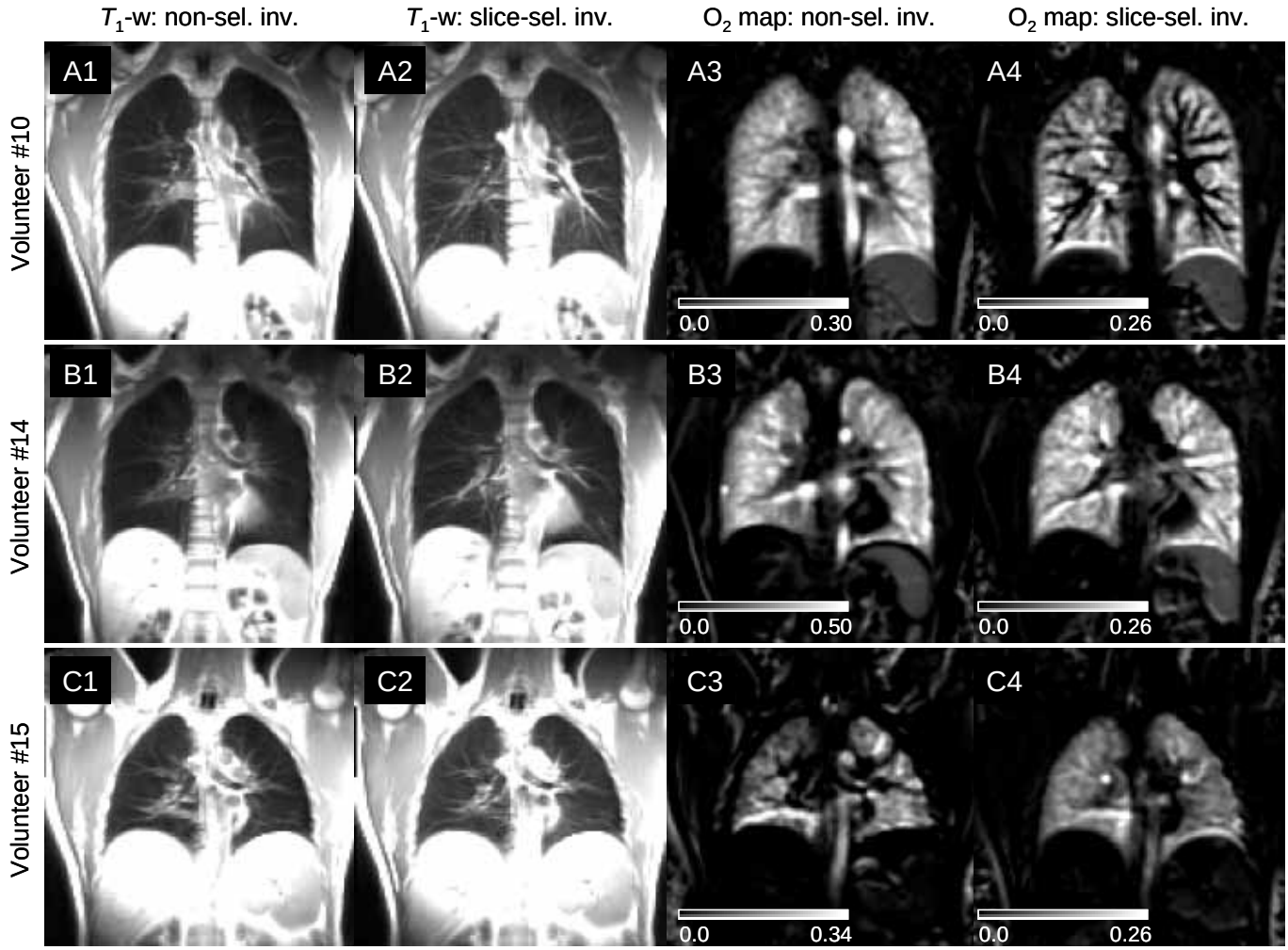

Figure 4: Comparison of non-selective and slice-selective inversion. Rows A, B, and C show data from volunteers #10, #14, and #15, respectively. T1-weighted images are presented in columns 1 (non-sel. inv.) and 2 (slice-sel. inv,); Maps of relative signal enhancement are shown in columns 3 (non-sel. inv.) and 4 (slice-sel. inv.). Note the differences in scaling of the maps in column 3.

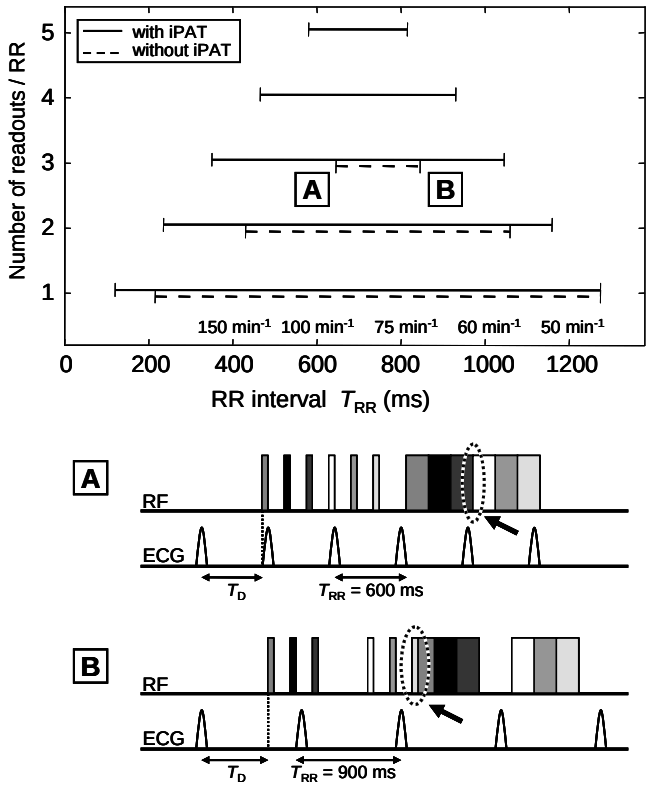

Figure 5: Ranges of RR intervals that are compatible with a certain number of readouts per cardiac cycle using the interleaved acquisition scheme. For shorter or longer RR intervals either the combined duration of the readouts becomes longer than T_{RR} (demonstrated in diagram A; the arrow points to the overlapping readouts) or the inversion pulses of the interleaved acquisitions collide with the subsequent acquisition (demonstrated in diagram B, the arrow points to the overlap of inversion pulse and readout). The RR interval ranges of the conventional sequence are drawn as dashed line, for the iPAT sequence as solid line. Note that the number of slices acquired in one respiratory cycle is twice the number of readouts per RR interval.

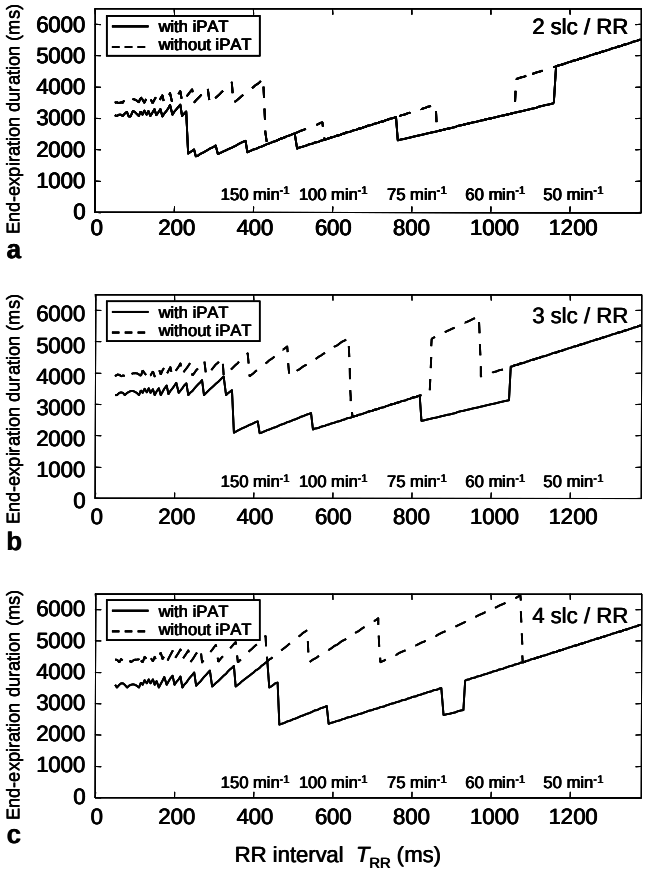

Figure 6: End-expiration duration T_{Exp} (see Fig. 1) required to avoid motion artifacts, shown for the conventional (dashed line) and iPAT acquisition (solid line). Steps in the data are caused by switching between the interleaved and non-interleaved acquisition scheme and by the varying numbers of heart beats between the first inversion pulse and the readout. (a) End-expiration duration for 2 slices per RR interval; (b) end-expiration duration for 3 slices per RR interval; (c) end-expiration duration for 4 slices per RR interval. Note that the number of slices acquired in one respiratory cycle is twice the number of readouts per RR interval.

Table 2: Comparison of non-selective and slice-selective inversion pulses.

	Non-selective inversion		Slice-selective inversion	
Volunteer	Relative signal increase	Std. dev. of relative signal increase	Relative signal increase	Std. dev. of relative signal increase
#10	16.8 %	6.5 %	10.7 %	8.3 %
#14	27.0 %	13.3 %	16.7 %	6.3 %
#15	10.9 %	10.0 %	11.1 %	4.5 %

The fraction of images accepted by the retrospective motion correction is very similar without and with iPAT as well (Table 1); the differences between the 3 acquisition schemes were not significant. There are large inter-individual variations of the number of accepted images; especially for volunteer #3, an extraordinary large number of acquisitions were discarded by the motion correction algorithm. This is also the only volunteer with a standard deviation of the signal increase larger than the actual increase (without and with iPAT), indicating a low data quality. In all other volunteers, the fraction of accepted acquisitions was greater than 50 %, and this number appeared sufficient for a reliable determination of the oxygen-induced signal increase.

Acquisitions were usually performed with the interleaved scheme; only in some volunteers with extraordinarily slow heart rate the triggering algorithm occasionally had to switch to the non-interleaved scheme (cf. Fig. 1). A more detailed computed analysis of the triggering algorithm and the sequence timing showed that an interleaved acquisition is possible for a much larger range of heart rates (RR intervals) with iPAT than without (see Fig. 5). For 4 slices (corresponding to 2 readouts in each diastolic interval) the interleaved acquisition without iPAT works for heart rates between 57/min and 140/min, but this range is considerably reduced for 6 slices (3 readouts in each diastolic interval). In this case, heart rates between 71/min and 93/min are required for an interleaved acquisition without iPAT, whereas with iPAT this range is increased to heart rates between 57/min and 170/min. Interleaved acquisitions of 8 or 10 slices are possible with iPAT only. Due to the automatic switching to the non-interleaved acquisition, the use of iPAT results in a decreased end-expiration duration T_{Exp} required for acquisitions without motion artifacts originating from diaphragm motion as shown in Fig. 6. The computations show that in particular for 3 and 4 slices per diastolic phase, the end-expiration duration is decreased from about 5 seconds without iPAT to less than 3 seconds with iPAT for the typical range of heart rates in patients and volunteers. For example, the acquisition of 6 slices with 3 slices per diastolic phase at a heart rate of 70/min requires an end-expiration duration of 5130 ms without iPAT and is reduced to 2565 ms with iPAT. Averaged over the range of typical heart rates between 60/min and 100/min, the mean end-expiration duration is 4112 ms (standard deviation 1045 ms) without iPAT and is significantly reduced to 2727 ms (257 ms) with iPAT ($p<0.001$, Wilcoxon two-sample test).

All data sets are based on the acquisition of 80 repetitions and thus the total time of acquisition was always 80 respiratory cycles (plus 1 additional cycle for the acquisition of reference scans when using iPAT). Since the respiration frequency varied inter-individually between about 6/min and 10/min, the total acquisition time varied as well between 8 and 13 minutes. All examinations were performed without any adverse reactions.

Discussion

In order to acquire multiple slices of T_1-weighted images per respiratory cycle, we implemented a slice-selective IR-HASTE sequence for oxygen-enhanced lung imaging with combined respiratory and ECG triggering. Optional parallel imaging support was added to accelerate the acquisition. The parallel acquisition technique provided advantages with respect to image quality and in particular for the sequence timing when combined with our triggering algorithm.

The double triggering scheme has been chosen to combine the advantages that recently have been described for both triggering methods applied separately in oxygen-enhanced lung MRI (10). In particular, identical diaphragm positions in all repetitions are important because the signal intensity of the lung parenchyma varies significantly during the respiratory phase (11) and this signal variation superimposes the oxygen-induced signal increase. By choosing end-expiration for image acquisition we could use the maximum lung signal and had the additional advantage that the diaphragm position is more uniform after expiration than after repeated inspirations (12). However, imaging in end-expiration requires some cooperation of the examined subjects; it turned out that a good verbal explanation and a short training scan substantially improved the cooperation during the acquisition. A second important factor influencing the acquisition quality is the end-expiration duration T_{Exp} that is required to perform inversion pulses and HASTE read-

outs for all slices. If this time period is sufficiently short, e.g. below 3 seconds, the examined subjects can breathe almost freely. These short end-expiration durations could be achieved when the timing parameters and especially the heart rate allowed for the interleaved acquisition scheme shown in Fig. 1a.

As has been shown in Fig. 5, the range of heart rates compatible with the interleaved readout is considerably extended when using parallel imaging. Thus, the required end-expiration time given in Fig. 6 can be significantly decreased by using iPAT. This allowed us to increase the number of coronal slices acquired in one respiratory cycle from 4 to 6 and thus to achieve a better coverage of the lung without increasing the required end-expiration time. This is especially important for patients who have difficulties with holding their breath in end-expiration for more than 3 seconds. Those patients benefit most from the application of the interleaved acquisition scheme and thus from using iPAT.

A potential problem of respiratory triggering is the variable T_R that can influence the degree of longitudinal relaxation at the following inversion and thus the signal intensity in the T1-weighted image. However, with typically 6 to 10 respiratory cycles per minute, the T_R varies between 6 and 10 seconds, i.e. between 5 T_1 and 8 T_1 in the lung parenchyma. Hence, the T_R is sufficiently long to provide an almost full relaxation to more than 99 % of the longitudinal equilibrium magnetization. The relatively low respiration rate of 6/min to 10/min most likely is a consequence of the instructions to the volunteers to breath deeply and slowly.

ECG triggering was used to position all HASTE readouts within the diastolic phase to avoid motion artifacts. Our triggering algorithm is based on a short time average of the heart frequency to extrapolate the timing of the four following R-waves. Although one might expect a certain variation in heart rate and therefore occasionally misplaced HASTE readouts with respect to the cardiac phase, motion artifacts were observed only rarely. The robustness of cardiac triggering can be improved by iPAT since the reduced echo train length enables us to position the readout in the diastolic phase with some safety delays after and before the enclosing R-waves. Thus, slight variations of heart rate will not lead to readouts during the R-wave. However, even with inserted safety delays the extrapolation of R-waves will be more critical in patients with arrhythmia. In this case it may be preferable to switch off the ECG triggering and use respiratory triggering only.

In our study, the combination of ECG and respiratory triggering worked robustly in all volunteers. The retrospective motion correction proved that in all volunteers except one the diaphragm position was within less than 1 pixel in typically 70 % to 100 % of all 80 repetitions. A further improvement of the acquisition may be achieved by online monitoring of the diaphragm position, e.g. with 2D navigator-based techniques. These methods promise higher accuracy of triggering than the mechanical respiratory belt. Adding an online evaluation of the image data immediately after the data acquisition, images with motion artifacts or shifted diaphragm position could be discarded and re-acquired in the next respiratory cycle. This should lead to more consistent data; however, at the cost of increased total acquisition time.

Visual evaluation of the T_1-weighted images showed a slightly improved image quality using iPAT. This can be explained by the shorter echo train length that reduces both motion during the readout and T_2-related blurring which is typical for HASTE acquisitions. Similar results have been reported by Heidemann et al. (13) for iPAT HASTE sequences applied without oxygen inhalation. As a further advantage of iPAT, the effective echo time could be decreased by almost 50 % to 11 ms. This combined with the reduced T_2 decay of the signal during the shortened readout seemed to compensate the iPAT-typical SNR loss such that no visible SNR difference with and without iPAT was observable. A quantitative evaluation of SNR was not performed because of the complex noise properties in iPAT images. Due to the iPAT post-processing, the noise is no longer distributed uniformly over the image but depends on the spatially varying geometry factor g (8). Therefore, noise may be lower in background regions than in the regions of interest and the conventional SNR determination must be expected to be inaccurate. Other methods to determine the SNR such as evaluating difference images (14) or series of repeated acquisitions are impaired by physiological signal variations such as varying posi-

tions or signals of vessels and are therefore not suitable for lung imaging either.

The oxygen-induced relative signal enhancement was not significantly different with and without iPAT in acquisition schemes 1 and 2; however, most volunteers examined with acquisition schemes 1 *and* 2 showed a higher signal increase with iPAT than without. We found a weakly significant difference of the signal enhancement in acquisition schemes 1 and 3. If this effect can be confirmed in further investigations, it may be explained by the reduced blurring artifacts with iPAT. Blurring propagates signal from muscle and fat tissue outside the lung into the lung, but this propagated signal is not enhanced by oxygen inhalation. Thus, the net effect is a reduced signal enhancement of the lung in images with increased blurring.

In comparison with other studies of oxygen-enhanced lung imaging, the main improvement of our IR-HASTE sequence is its ability to acquire multiple slices in a comparably short time. This has been achieved by slice-selective inversion and refocusing pulses and interleaving of inversion and readout. Most other groups that we are aware of have worked with non-selective inversion or refocusing pulses (15–17). Publications by Ohno et al. (4, 5) do not contain details about slice-selective or non-selective inversion or total examination time. A potential disadvantage of using slice-selective inversion may be an increased sensitivity to perfusion: the signal within the slice will be influenced by inflowing non-inverted spins from outside the slice. To minimize this effect, the thickness of the inverted slice was chosen twice as large (16 mm) as the thickness of the image slice (8 mm).

Our direct comparison of non-selective inversion and slice-selective inversion with doubled inversion slice thickness demonstrated that similar results can be obtained with both techniques. After slice-selective preparation, the T_1-weighted images showed signal enhancement in the pulmonary vessels that can be interpreted as inflow of non-prepared spins. However, a very similar enhancement was also seen after non-selective inversion, indicating that a certain contamination with non-inverted spins is unavoidable at inversion times of 1300 ms. Several studies with non-selective inversion have demonstrated the feasibility of oxygen-enhanced MRI with comparable inversion times in spite of this inflow effect (6, 15, 17).

The calculated maps of relative signal increase showed the most substantial differences with respect to the signal within the pulmonary vessels. This signal was reduced after *slice*-selective inversion in volunteer #10, and after *non*-selective inversion in volunteer #15; these disagreeing results may be explained by different pulmonary circulation parameters and the exact position of the readout within the cardiac cycle. However, the signal increase in the large pulmonary vessels is less important for evaluation of the lung function than the signal in the lung parenchyma which was very similar for both techniques in volunteers #10 and #15. In volunteer #14, the spatial pattern of signal enhancement was very similar with both techniques as well, but the absolute increase was reduced by almost 40 % after slice-selective preparation. Again this may be explained by the inflow of non-inverted spins that are distributed much more homogeneously in the lung than in the two other volunteers. This effect reduces slightly the image quality of the calculated maps; however, the analysis of the maps based on the local signal distribution is not substantially influenced as long as the (differently scaled) maps remain very similar.

In general, the proposed technique is aimed on a semi-quantitative evaluation by comparing the signal increase in different areas of the lung parenchyma of a patient or by calculating parameters that describe the homogeneity or inhomogeneity of the signal increase such as the spatial standard deviation of the signal increase. Therefore, a comparable signal change in all slices of a single measurement is desirable whereas the absolute value of the signal increase is less important. This is achieved by acquiring slices with identical inversion times rather than applying a single non-selective inversion pulse before the readout of multiple slices. In the latter case, the non-selective inversion might be advantageous for the signal quality; however, the inversion times will be different for all acquired slices and therefore a semi-quantitative comparison of data of different slices will not longer be possible. A third method, the repeated application of a non-selective prepared single slice experiment is not compatible with the requirement of a moderate measurement duration that enables us to combine oxygen-enhanced imaging with other MRI techniques.

The application of inversion pulses with doubled slice thickness required a gap between the slices to

avoid overlapping of adjacent inversion slices. Expecting non-perfect inversion slice profiles, we chose a slice distance of 24 mm center-to-center; however, this distance may be decreased in future studies down to 16 mm. If a complete coverage of the lung without any gaps is desired, the entire measurement could either be repeated with shifted slice positions that cover the gaps of the prior experiment, or the additional slices could be acquired alternating with the original ones, thus increasing the block duration of the application of room air and oxygen, respectively. With both strategies, the total measurement duration would be increased by a factor of 2 or 3 depending on the original slice distance.

This is the first study to our knowledge with combined respiratory and ECG triggering for oxygen-enhanced lung MRI; other groups have used no triggering at all or only one physiological signal. The latter strategy has been realized by cardiac triggering and data acquisition during free breathing or breath hold periods (6, 10, 15), or by respiratory triggering only (5, 10).

Due to the high performance of our gradient system we could achieve a very short echo spacing of 2.7 ms. This in combination with iPAT reduced the minimum echo time to 11 ms in spite of the linear k-space sampling in phase-encoding direction. Since linearly acquired data is generally less affected by blurring than data acquired with centric k-space reordering due to the shorter interval between the sampling of adjacent lines and, thus, an improved point-spread function, we preferred the linear acquisition scheme. The inversion time of 1300 ms was similar to the one used by Mai et al. (15) and close to the theoretical optimum (3). Inversion preparation with shorter inversion times have been used in other studies (5, 10, 18) and further investigations must show whether they provide advantages in multi-slice imaging because of a potentially reduced inflow of non-inverted spins.

To analyze the signal time course we simply calculated the relative signal increase after discarding data reflecting the wash-in and wash-out of oxygen. This simple strategy was used because our study was focused on the acquisition technique rather than on data evaluation or clinical application. More elaborate data evaluation will be used in future studies including calculation of the signal slope after changing the gas supply (6) or correlation analysis using the complete signal time course (15).

In conclusion, using slice-selective pulses, parallel imaging, and combined respiratory and ECG triggering, oxygen-enhanced lung MRI with acquisition of 6 slices and 80 repetitions can be performed in 8 to 13 minutes depending only on the respiratory frequency of the examined subject. Thus, oxygen-enhanced lung imaging becomes sufficiently fast to be inserted into a clinical routine MRI examination of the lung consisting of other morphologic and functional methods such as lung perfusion MRI and pulmonary MR angiography.

Acknowledgements

We would like to thank Berthold Kiefer, Mathias Nittka, and Bernd Kuehn (Siemens Medical Solutions) for their technical support in MR pulse sequence development. Furthermore, we are very grateful to Michael Gießel and Thomas Seitz from the technical anesthesia department (University of Munich) for their support in constructing the oxygen applicator system.
This work was supported by the Deutsche Forschungsgemeinschaft, Grant Nos. SCHE 319/6-1 and PE 925/1-3.

References

[1] Edelman RR, Hatabu H, Tadamura E, Li W, Prasad PV. Noninvasive assessment of regional ventilation in the human lung using oxygen-enhanced magnetic resonance imaging. Nat Med 1996;2:1236–1239.

[2] Chen Q, Jakob PM, Griswold MA, Levin DL, Hatabu H, Edelman RR. Oxygen enhanced MR ventilation imaging of the lung. MAGMA 1998;7:153–161.

[3] Löffler R, Müller CJ, Peller M, Penzkofer H, Deimling M, Schwaiblmair M, Scheidler J, Reiser M. Optimization and evaluation of the signal intensity change in multisection oxygen-enhanced MR lung imaging. Magn Reson Med 2000;43:860–866.

[4] Ohno Y, Hatabu H, Takenaka D, Adachi S, Van Cauteren M, Sugimura K. Oxygen-enhanced MR ventilation imaging of the lung: preliminary clinical experience in 25 subjects. AJR Am J Roentgenol 2001;177:185–194.

[5] Ohno Y, Hatabu H, Takenaka D, Van Cauteren M, Fujii M, Sugimura K. Dynamic oxygen-enhanced MRI reflects diffusing capacity of the lung. Magn Reson Med 2002;47:1139–1144.

[6] Müller CJ, Schwaiblmair M, Scheidler J, Deimling M, Weber J, Löffler RB, Reiser MF. Pulmonary diffusing capacity: assessment with oxygen-enhanced lung MR imaging preliminary findings. Radiology 2002;222:499–506.

[7] Sodickson DK, Manning WJ. Simultaneous acquisition of spatial harmonics (SMASH): fast imaging with radiofrequency coil arrays. Magn Reson Med 1997;38:591–603.

[8] Pruessmann KP, Weiger M, Scheidegger MB, Boesiger P. SENSE: sensitivity encoding for fast MRI. Magn Reson Med 1999;42:952–962.

[9] Griswold MA, Jakob PM, Heidemann RM, Nittka M, Jellus V, Wang J, Kiefer B, Haase A. Generalized autocalibrating partially parallel acquisitions (GRAPPA). Magn Reson Med 2002;47:1202–1210.

[10] Vaninbroukx J, Bosmans H, Sunaert S, Demedts M, Delcroix M, Marchal G, Verschakelen J. The use of ECG and respiratory triggering to improve the sensitivity of oxygen-enhanced proton MRI of lung ventilation. Eur Radiol 2003;13:1260–1265.

[11] Mai VM, Chen Q, Li W, Hatabu H, Edelman RR. Effect of respiratory phases on MR lung signal intensity and lung conspicuity using segmented multiple inversion recovery turbo spin echo (MIR-TSE). Magn Reson Med 2000;43:760–763.

[12] Losert C, Nikolaou K, Scheidler J, Mueller CJ, Schwaiblmair M, Reiser MF. Optimized respiratory and ECG gating in oxygen-enhanced MR ventilation imaging of the lung. Proc Intl Soc Mag Reson Med 2002;10:1971.

[13] Heidemann RM, Griswold MA, Kiefer B, Nittka M, Wang J, Jellus V, Jakob PM. Resolution enhancement in lung 1H imaging using parallel imaging methods. Magn Reson Med 2003;49:391–394.

[14] Firbank MJ, Coulthard A, Harrison RM, Williams ED. A comparison of two methods for measuring the signal to noise ratio on MR images. Phys Med Biol 1999;44:N261–N264.

[15] Mai VM, Tutton S, Prasad PV, Chen Q, Li W, Chen C, Liu B, Polzin J, Kurucay S, Edelman RR. Computing oxygen-enhanced ventilation maps using correlation analysis. Magn Reson Med 2003;49:591–594.

[16] Jakob PM, Hillenbrand CM, Wang T, Schultz G, Hahn D, Haase A. Rapid quantitative lung (1)H T(1) mapping. J Magn Reson Imaging 2001;14:795–799.

[17] Nakagawa T, Sakuma H, Murashima S, Ishida N, Matsumura K, Takeda K. Pulmonary ventilation-perfusion MR imaging in clinical patients. J Magn Reson Imaging 2001;14:419–424.

[18] Hatabu H, Tadamura E, Chen Q, Stock KW, Li W, Prasad PV, Edelman RR. Pulmonary ventilation: dynamic MRI with inhalation of molecular oxygen. Eur J Radiol 2001;37:172–178.